

Computational modeling of size effects in concrete specimens under uniaxial tension

Miroslav Vořechovský · Václav Sadílek

Received: 14 April 2008 / Accepted: 14 January 2009 / Published online: 10 February 2009
© Springer Science+Business Media B.V. 2009

Abstract The paper presents a follow-up study of numerical modeling of complicated interplay of size effects in concrete structures. The major motivation is to identify and study interplay of several scaling lengths stemming from the material, boundary conditions and geometry. Methods of stochastic nonlinear fracture mechanics are used to model the well published results of direct tensile tests of dog-bone specimens with rotating boundary conditions. Firstly, the specimens are modeled using microplane material and also fracture-plastic material laws to show that a portion of the dependence of nominal strength on structural size can be explained deterministically. However, it is clear that more sources of size effect play a part, and we consider two of them. Namely, we model local material strength using an autocorrelated random field attempting to capture a statistical part of the combined size effect, scatter inclusive. In addition, the strength drop noticeable with small specimens which was obtained in the experiments could be explained either by the presence of a weak surface layer of constant thickness (caused e.g. by drying, surface damage, aggregate size limitation at the boundary, or other irregularities) or three dimensional effects incorporated by out-of-plane flexure of specimens. The latter effect is examined by comparison of 2D and 3D models with the same material laws. All three named sources

(deterministic-energetic, statistical size effects and the weak layer effect) are believed to be the sources most contributing to the observed strength size effect; the model combining all of them is capable of reproducing the measured data. The computational approach represents a marriage of advanced computational nonlinear fracture mechanics with simulation techniques for random fields representing spatially varying material properties. Using a numerical example, we document how different sources of size effects detrimental to strength can interact and result in relatively complicated quasibrittle failure processes. The presented study documents the well known fact that the experimental determination of material parameters (needed for the rational and safe design of structures) is very complicated for quasibrittle materials such as concrete.

Keywords Size effect · Scaling · Random field · Weak boundary · Crack band · Dog-bone specimens · Quasibrittle failure · Crack initiation · Stochastic simulation · Characteristic length · Weibull integral · Microplane model · Fracture-plastic model

1 Introduction

This paper studies interacting size effects on the nominal strength of concrete structures using a combination of finite element software enabling nonlinear analyses and probabilistic methods. The target is to identify possible sources of size effect, study them and model

M. Vořechovský (✉) · V. Sadílek
Institute of Structural Mechanics, Brno University
of Technology, Veveří 95, 602 00 Brno, Czech Republic
e-mail: vorechovsky.m@fce.vutbr.cz

them together in one complex model. We want to show how the different sources interact with each other. We are particularly interested in the interaction of different material length scales and the effect of such interaction on strength size effect.

The work is related to previous papers by other authors among which the most influential is the work by [Gutiérrez and de Borst \(2002\)](#), dealing with deterministic and statistical lengths and their role in size effect. Several very influential works were produced in the 1990s; [Carmeliet and Hens \(1994\)](#) and [Carmeliet and de Borst \(1995\)](#). They combined a simple non-local damage model and simulation of a bi-variate random field of material properties (damage threshold and strain softening) within a single finite element computational model, and studied the two different length parameters: the characteristic length of the nonlocal damage model, and the correlation distance for the random field. The illustrated example presenting finite-element analyses of direct-tension tests has shown that the specimen exhibits structural behavior that is representative of nonsymmetrical deformation, with a nonlinear stress-displacement curve. It has also shown that the two sources of size effect can be modeled satisfactorily well. Their model utilizes experience gained from a paper by [Mazars et al. \(1991\)](#), who also studied the two sources of size effect in cementitious materials using a continuous damage model, and compared the results with experiments on both notched and unnotched bending beams. Unfortunately, they did not consider more than one random property, and ignored its spatial correlation. The interplay of deterministic and statistical size effects is one of the central topics in PhD thesis by [Vořechovský \(2004b\)](#). Some analytical results supported by a large computational case study of the

Malpasset dam failure are published by [Vořechovský et al. \(2005\)](#), [Bažant et al. \(2007b\)](#).

Even though we have the ambition to study the size effect phenomena in general terms, we have decided to illustrate the problem using a particular example for the sake of easier comprehension and transparency. In particular, we numerically study the well published experimental results of direct tensile tests on dog-bone specimens with rotating boundary conditions of varying size (size range 1:32) performed by van Vliet and van Mier and summarized in the PhD thesis by [van Vliet \(2000\)](#) and in papers by [van Vliet and van Mier \(1998, 1999, 2000a,b\)](#), [van Mier and van Vliet \(2003\)](#), [Dyskin et al. \(2001\)](#). We are interested in the series of “dry” concrete specimens A to F (dimension D varying from 50 to 1,600 mm, see Fig. 1 and Table 1); a series accompanied by tensile splitting verification tests. The paper attempts an explanation of the interacting size effects on the mean and variance of nominal strength by a combination of random field simulation of local material properties and “weak boundary” effects, and a nonlinear fracture mechanics simulation based on a cohesive crack model. There has been much effort expended on different explanations of the experimentally obtained size effects on strength from several different points of view. Firstly, the effect of a non-uniform distribution of strains in the smallest cross-section was studied using simple linear constitutive law ([van Vliet and van Mier 1999, 2000a](#)), and a separation of structural and material size effects was discussed. [Van Vliet and van Mier \(1999\)](#) argue that most of the experimentally observed size effect could be explained by strain/stress gradients that develop due to several reasons. The results were also compared to the Weibull theory ([Weibull 1939](#)) based on the weakest-link model which was found to

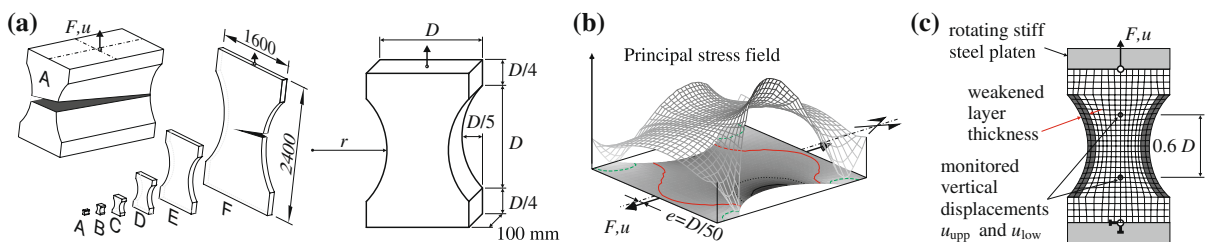


Fig. 1 (a) Dog-bone series (specimens A to F) tested by [van Vliet and van Mier \(1998\)](#); (b) elastic principal stress field; (c) 2D model in ATENA software with a surface layer. Strain

ε is calculated using the separation $\Delta u = u_{\text{upp}} - u_{\text{low}}$ of two points over the control length $l_c = 0.6D$

Table 1 Experimental data. Specimens' dimensions, nominal strengths, sample size, c.o.v. and corresponding Weibull modulus m

	D (mm)	$r = 0.725D$ (mm)	σ_N mean (std. dev.) (MPa)	Specimens (#)	c.o.v [%] (shape par.)
A	50	36.25	2.54 (0.41)	10	16.2 (7.27)
B	100	72.5	2.97 (0.19)	4	6.28 (19.7)
C	200	145	2.75 (0.21)	7	7.67 (16.0)
D	400	290	2.30 (0.09)	5	4.02 (31.1)
E	800	580	2.07 (0.12)	4	5.91 (21.0)
F	1600	1160	1.86 (0.16)	4	8.67 (14.1)

fit the mean nominal strength of sizes B to F (van Vliet and van Mier 1998, 1999, 2000a,b, van Mier and van Vliet 2003). The slope of the mean size effect curve corresponds to a Weibull modulus of 12, which does not coincide exactly with the measured scatter of strengths at each size. However, this is required in the Weibull type of size effect. Secondly, the effect of Gaussian stress fluctuation with non-uniform loading was studied by Dyskin et al. (2001), and the developed model, employing a limiting distribution of independent Gaussian variables with linear trend, agrees with the experimental data very well. Van Mier and van Vliet also compared the data to the “Delft lattice model” using a simple local elastic-brittle material with both regular and random lattices, and they obtained good results. The statistical part of experimentally obtained size effect has also been modeled by Lehký and Novák (2002), employing a limiting distribution of independent Weibull variables describing the distribution of strength.

The present work extends a previous work presented by Vořechovský (2007) in several ways. In this paper, we firstly try to explain the mean size effect curve with deterministic effects (not taking into account the local material strength with a random field). To do so, two material laws are compared, namely the micro-plane material model and fracture-plastic model implemented as NLCEM model in ATENA software (Červenka and Pukl 2005). There is a partial explanation of the decreasing slope of the mean size effect curve (MSEC) in a double-logarithmic plot (nominal strength versus characteristic size). However, the strong decrease in the mean strength of the smallest specimen A is believed to be sufficiently captured by a modeled weak surface layer with a thickness of about 2 mm. A parametric study of the influence of “weak layer” thickness and the percentage reduction in the layer’s

strength compared to the bulk strength was presented by Vořechovský (2007). Next, we approximate the local material strength via an autocorrelated random field, attempting to capture the statistical size effect, scatter inclusive, and finally combine all sources together. All above named studies are performed in two dimensions. In order to quantify possible effects of out-of-plane flexure we have performed three dimensional modeling taking into account the reported non-uniformity of stiffness over the specimens’ width.

2 Experiments

The experiments by van Vliet and van Mier are well documented in the seven references cited in the introduction. We will briefly mention only those necessary data needed to explain the computational model: all other details can be found in the cited publications. Dog-bone shaped specimens were loaded in uniaxial tension with geometrically scaled eccentricity from the vertical axis of symmetry $e = D/50$. The loading platens were allowed to rotate freely in all directions around the loading points at the top and bottom concrete faces. The loading platens were glued to the concrete. Six different sizes were tested; all specimens were geometrically similar (see Fig. 1a). The specimen thickness was kept constant ($b = 0.1$ m), implying a transition from plane strain like conditions at the smallest size to plane stress conditions for the large sizes. The concrete mixture was reported to have an average cube compressive strength of 50 MPa and a maximum aggregate size $d_{\max} = 8$ mm.

For comparative purposes, it is necessary to define a nominal strength σ_N . Since the eccentricity of the loading points has been geometrically scaled in both experiments and numerical models, we can ignore its effect on

the linear state stress field and define the nominal stress σ simply as a function of the characteristic dimension D (maximum specimen width), instantaneous tensile force F applied at the concrete faces at the eccentricity e and the cross sectional area in the middle of the specimen A ($= 0.6Db = 0.06Dm^2$):

$$\sigma = \frac{F}{A} \quad (1)$$

Having defined the nominal stress, we define the nominal strength σ_N as the nominal stress attained at maximum loading force ($\sigma_N = F_{\max}/A$).

Note that the smallest specimen size **A** has a width in the ‘neck-area’ of only 30 mm. Compared to the maximum aggregate size of 8 mm, it must be questioned whether such a small specimen (being too small in size to be considered a representative volume element) can still be treated identically to the rest of the series.

The authors of experiments have reported that specimens were casted such that, during manufacturing of specimens, the back surfaces were at bottom (mould side) and that casting took place in three layers [van Vliet and van Mier \(1999\)](#). This procedure is likely to induce stiffness differences in the direction of casting which could be more pronounced in relatively thick small specimens rather than in large specimens, see specimen **A** in [Fig. 1a](#) and [Fig. 6](#) right.

3 The deterministic models

3.1 Two-dimensional modeling

Most of the present studies were performed with 2D models. We start with microplane modeling and compare the results to fracture-plastic models later on.

A strong contribution to the non-uniformity of the nominal strength is the “energetic-deterministic” size effect caused by an approximately constant fracture process zone (FPZ) size with stress redistribution in specimens of all sizes; see e.g. [Bažant and Planas \(1998\)](#). This effect can be modeled e.g. by the finite element method provided that the fracture energy and the whole shape of pre- and post-peak behavior is correctly introduced. We created the deterministic model in the ATENA software package ([Červenka and Pukl 2005](#)), using Bažant’s microplane material model (version 4) ([Bažant et al. 2000](#)) and the crack band model ([Bažant and Oh 1983](#)) as a simple regularization. The

basic idea of the crack band model for strain-softening in tension (and also of the model of [Pietruszczak and Mróz \(1981\)](#) for strain-softening in shear) is to modify the material parameters controlling the smeared cracking such that the energies dissipated by large and small elements per unit area of the crack band would be identical. The choice of the microplane constitutive model is supported by the fact that M4 seems to be the best model able to capture the complex behavior of concrete under general conditions. The crack band model has been chosen as the only technique widely used and incorporated in commercial codes due to its simplicity. The M4 microplane model does not explicitly work with strain decomposition into elastic and inelastic parts and therefore the so-called equivalent localization element ([Červenka et al. 2005](#)) has been implemented into ATENA. This technique removes the problem of the spurious mesh size dependence of the results, while a certain dependence on the mesh orientation still remains (for a concise overview of various numerical methods and their ability to analyse localization and failure in engineering materials see [de Borst et al. \(2004\)](#)).

Specimens were loaded by deformation increments and the force F was monitored, see [Fig. 1c](#). We ignored the transition from plane strain to plane stress conditions with growing specimen size in two-dimensional models where we have modeled the whole series of sizes with a plane stress model. Verifications using three dimensional models follow. Based on the information about the average cube compressive strength of 50 MPa, ATENA generated a set of consistent microplane parameters: $K1 = 1.5644 \cdot 10^{-4}$, $K2 = 500$, $K3 = 15$, $K4 = 150$ ([Caner and Bažant 2000](#)), crack band $c_b = 30$ mm, number of microplanes 21 (an efficient formula that still yields acceptable accuracy involves 21 microplanes to integrate over a sphere ([Bažant and Oh 1986](#))). The parameters K1 through K4 are phenomenological microplane model parameters and they do not have a physical meaning; they can be understood as scaling parameters of given curve shapes (criteria) describing the so-called “boundaries”. Briefly, K1 plays a role in relations for the tensile normal boundary (needed for tensile cracking, fragment pullout and crack closing), and also compressive deviatoric and tensile deviatoric boundaries (spreading and splitting); K1 and K2 affect shear boundary (friction); K1, K3 and K4 are present in the relations for both tensile and compressive volumetric boundaries (pore

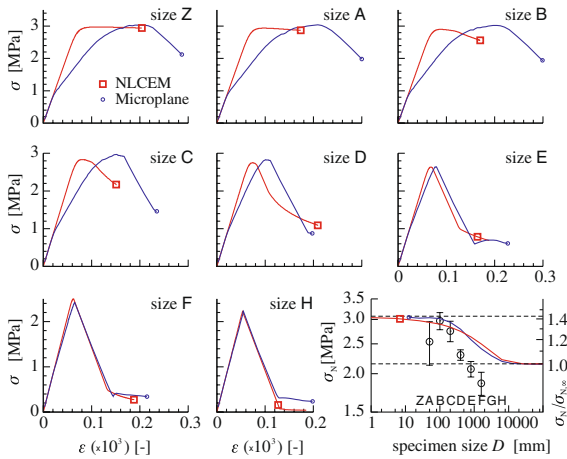


Fig. 2 Comparison of deterministic nominal stress-strain diagrams obtained with microplane model and fracture-plastic model for a range of structure sizes. Bottom right: nominal strength dependence on structure size obtained with the two material models compared to experiment average strengths with errorbars

collapse, expansive breakup); for a full description see Bažant et al. (2000).

We changed the crack band to 8 mm, a value that enables us to explain most of the experimentally obtained size effect, see Fig. 2 bottom right. The crack band size is related to the fracture energy of the material and controls the size at which the continuum computational model undergoes transition from relatively ductile to elastic-brittle failure (transition between two horizontal asymptotes in the size effect plot, see Fig. 2 bottom right). By varying the strength related parameter K_I (while keeping the characteristic length ℓ_{ch} or c_b constant), the whole curve moves up and down as a rigid body. Another noticeable fact is that in the size effect plot the curve can be shifted right or left as a rigid body just by changing c_b . More specifically, the deterministic nominal strength computed for a certain size of D using a c_b value is also the nominal strength of size sD computed with crack band width $s c_b$ (s is a positive scaling parameter):

$$\text{for } \forall s > 0: \sigma_N^{\text{det}}(D, c_b) = \sigma_N^{\text{det}}(sD, s c_b) \quad (2)$$

This has a direct implication noticed already by other authors before for the case of a fictitious crack (Bažant and Planas 1998): the nominal structural strength depends, when all other parameters are fixed, on the dimensionless ratio of D and ℓ_{ch} . The fictitious crack can be shown to be equivalent to the smeared crack

band model for mode I fracture under consideration (see Bažant and Planas 1998, p. 255). The characteristic length ℓ_{ch} has a linear relationship with the crack band width c_b (Bažant and Planas 1998). In our case, therefore, we can write that the nominal strength is proportional to the tensile strength times a function of the ratio between D and ℓ_{ch} ; a fact exploited in Eq. 4 and discussed later on in this paper. It should not remain unnoticed that Eq. 2 has a direct relation to the Vashy-Buckingham Π -theorem (Vashy 1892, Buckingham 1914) on dimensional analysis (see e.g. Barenblatt 1996). It turns out that, when the ratio between D and c_b (or ℓ_{ch}) is close to unity, the structure is in transition between two important asymptotes: plastic and elastic solutions. More precisely, if the structure is much smaller than ℓ_{ch} ($D/c_b \rightarrow 0$), the behavior is fully elastic-plastic and can be simply predicted based on the knowledge of direct tensile strength f_t (the yielding point in this case). On the other hand, if the structural size D is much larger compared to c_b (or ℓ_{ch}), the behavior is linear elastic with a sudden failure at the onset of reaching the direct tensile strength f_t at any point in the material, see e.g. Vořechovský et al. (2005), Bažant et al. (2007b). In this case, what matters is the profile of principal tensile stresses over the structure, see Fig. 1b.

From this we can also deduce the value of $\sigma_N(\infty, c_b) \equiv \sigma_{N,\infty}$, it being the large size asymptote in Fig. 2 bottom right. Simply, it is the nominal stress when the extreme principal tension reaches the direct tensile strength f_t . Note that in the definition of σ_N the eccentricity of loading and possible stress concentration in the specimen’s neck are not reflected and therefore $f_t \neq \sigma_{N,\infty}$. The ratio of $f_t/\sigma_{N,\infty}$ can be deduced by considering two effects: (i) stress concentration due to curved sides of the specimens and, (ii) eccentricity of the loading force. The first factor equals 1.24 (ratio between the maximum stress attained at the curved boundary and a remote uniform stress). The second factor of 1.2 can be computed from normal stress due to centric normal force plus bending moment $= F/A(1 + 6e/0.6D) = F/A(1 + 0.2)$. The multiple of these two factors $1.24 \times 1.2 = 1.49$ agrees well with FEM simulations of the eccentrically loaded large sized specimens giving $f_t/\sigma_{N,\infty} = 1.49$.

Regarding the asymptotic strength of small specimens $\sigma_N(0, c_b) \equiv \sigma_{N,0}$ one can argue that a specimen made of ideal elastic-plastic material reaches its maximum force when the whole neck cross section is

yielding (at stress equal to f_t). Therefore the theoretical limit nominal strength equals f_t , no matter the eccentricity and the curved shape. Our FEM simulations with both microplane and NLCEM models predict the maximum nominal stress of small specimens at $\sigma_{N,0} \approx 0.95 f_t = 1.42 \sigma_{N,\infty}$. This value is, at the same time, the maximum size effect that can be captured deterministically by considering stress redistribution ($\approx 42\%$ reserve), see the right hand ordinate in Fig. 2.

In order to compare the way microplane model captures the energetic-deterministic size effect due to stress distribution, we performed a parallel study with the fracture-plastic model named ‘NLCEM’ (nonlinear cementitious) in ATENA software. In this model the conventional parameters are used to define a material law. The most relevant are: the cube compressive strength of 50 MPa (we have set it equal to the one in microplane model and used it to generate the implicit values for the rest of the material parameters applied in the integration points mentioned next), uniaxial compressive strength $f_c = 42.5$ MPa, modulus of elasticity E (set to 36.95 GPa such that the stiffness initial of microplane model and NLCEM models were equal), uniaxial tensile strength $f_t = 3.2$ MPa, fracture energy $G_F = 200$ N/m (exponential crack opening obtained experimentally by Hordijk 1991). Using this set of material parameters we have performed deterministic computations with a wide range of structure sizes (overlapping the tested range). Comparison of stress-strain diagrams obtained with the two material models is presented in Fig. 2 together with the size effect plot in the transition zone. It can be seen that the overall ideal plastic behavior is the limiting behavior for the smallest specimens while elastic-brittle-like curves are obtained for the large sizes. Note, that the transition is different with NLCEM and microplane models. When the structural size is very small, microplane model predicts strong pre-peak stiffness reduction even though the initial stiffness is equal to the one in NLCEM material model. The large size asymptotic strength is equal for both models and so does the small size asymptotic strength. The transition though is slightly different and depends on the boundaries in microplane model and crack-opening curve with other material parameters in NLCEM model.

The role of fracture energy in NLCEM model for scaling of structural strength is very similar to the role of crack band in the microplane model in Eq. 2. It can be easily checked that, for fixed E and f_t :

$$\text{for } \forall s > 0: \sigma_N^{\text{det}}(D, G_F) = \sigma_N^{\text{det}}(sD, sG_F) \quad (3)$$

It is because the Irwin’s characteristic length $\ell_{\text{ch}} = E G_F / f_t^2$ scales linearly with G_F and therefore varying G_F is equivalent to varying ℓ_{ch} . In other words, the size effect plot in Fig. 2 bottom right can be shifted right or left as a rigid body just by changing G_F : $\sigma_N^{\text{det}}(D, G_F/s) = \sigma_N^{\text{det}}(sD, G_F)$, see Fig. 4. Not only the nominal strength is equal for the scaled structure. If both the structure size and fracture energy in NLCEM model are scaled s times, the stress and displacement fields take the same values over the scaled coordinates. The same was true in the case of microplane modeling: if both the structure and crack band width is scaled s times, the stress and displacement fields take the same values over the scaled coordinates. This fact simplifies the preprocessing of numerical models of a size effect series: simply create a model of one size only and vary G_F (or c_b) instead of D .

3.2 Effect of varied G_F and c_b at element and structural levels

We have performed simple numerical experiments with ATENA software using which we document the effects of varied G_F and c_b on tensile response of (i) one element and (ii) dog-bone specimens.

Fig. 3 presents stress-strain (force-displacement) diagrams of one square finite element of unit size loaded in uniaxial tension. The top row shows the situation with NLCEM model, in which the original fracture energy $G_F = 2,000$ N/m is multiplied by several factors s ranging from 1/20 to 10 (f_t and E were kept constant at values mentioned above). The bottom row shows a similar numerical experiment in microplane model with original crack band width $c_b = 30$ mm multiplied by factors s ranging from 1/10 to 32 (again, the other parameters were kept as before). It is known (see e.g. Bažant and Planas 1998) that when using the crack band technology, the finite element can be imagined to consist of an inelastic part with softening behavior and a perfectly elastic spring coupled in a series (see Fig. 3 top left). It can be seen that both the initial (spring) stiffness E and tensile strength are not affected by variations of G_F or c_b . The area below the curves is almost perfectly proportional to the scaling factor s (see the right hand side plots in Fig. 3 of stress against scaled inelastic strains, that collapse into one curve). There is one condition, though, for the scalability of

fracture energy, that is thoroughly described in sect. 8.6.4 of [Bažant and Planas \(1998\)](#): the finite element can not be arbitrarily large compared to the characteristic length (or c_b). Or, equivalently in NLCEM model, the fracture energy of a single finite element must be greater than the elastic strain energy accumulated in the spring at the peak stress: $G_F^{(E)} > f_t^2/(2E)$. The problem is that snap-back behavior can not be captured by the nodal displacement controlled computation. Therefore, one can see that when s is small in the two material models, the finite elements dissipate more energy than they should. If no other criterion (such as those recommended in [Bažant and Planas \(1998\)](#), sect. 8.6) can be implemented in the finite element program used, caution must be paid that the element fracture energy of the crack band is greater than the elastic energy of the spring. The finite element fracture energy in our case is simply $G_F^{(E)} = G_F/L^{(E)}$, where $L^{(E)}$ is the width of elements perpendicular to the direction of cracking. We have checked that this criterion was fulfilled in all dog bone models studied in this paper. This was one important limitation when exploiting Eqs. 2 and 3 for the simplified modeling of size effect tests and applies to modeling of very large structures using the reference sized model with an identical mesh (and with reduced $G_F [c_b]$ in NLCEM [microplane] model respectively).

Another limitation when using the reference size to mimic a very large size is that if the numerical mesh is kept in the whole series, the resolution of stresses (e.g. in the fracture process zone) might become insufficient.

Since the dog bone specimens are not loaded just by uniform tension, stress redistribution can take place. It was concluded that varying fracture energy (or crack band width) is in fact equivalent to varying the proportion between structural size and characteristic length (characterizing the material heterogeneity scale). In order to document this numerically using the dog bone specimens models, we have varied the fracture energy G_F by multiplying it with parameter s ($s = 2, 4, 8, 16, 32$ and their inverses, the largest to the smallest ratio equals 1:1,024) and plotted the nominal strength of specimens as a representative parameter against the structural size (which was kept constant). If we, however, shift the points towards the size D/s , the points fall exactly on the size effect curve computed with a constant G_F and varied size D , see Fig. 4. The nominal strength dependence on size in the studied case of dog-bone specimens for instance, can be fitted very well with the following formula ([Bažant and Planas 1998](#)):

$$\sigma_N^{det}(D) = \sigma_{N,\infty} \left(1 + \frac{D_b}{D + l_p} \right) \tag{4}$$

where, aside from $D_b \approx 300$ mm, l_p is a second deterministic characteristic length controlling the center of transition to the left ‘plastic’ horizontal asymptote. The value of l_p can be deduced from the ratio of ‘ideal-plastic’ limiting strength and ‘elastic-brittle’ limiting strength $\eta_p = (1 + D_b/l_p) \approx 1.42$; therefore $l_p \approx 714$ mm (which happens to be quite close to the Irwin’s characteristic length $\ell_{ch} = E G_F/f_t^2 \approx 720$ mm). Formula (4) gives the transition from perfectly plastic behavior for $D/l_p \rightarrow 0$ (corresponding to an elastic body in which the crack is filled with a perfectly plastic glue), through quasibrittle behavior, to perfectly brittle behavior for $D/D_b \rightarrow \infty$. For the meaning of the parameters and justification of the formula, the reader is referred e.g. to [Bažant et al. \(2007b\)](#) and references therein.

It is an occasional practise to study a random model response of structures with varied (randomized) fracture energy (keeping an identical crack opening law curve shape). If the size effect relation such as the one in Eq. 4 is known, the probabilistic distribution of random strength σ_N for a given size D can be written analytically just using a random variable transformation. The

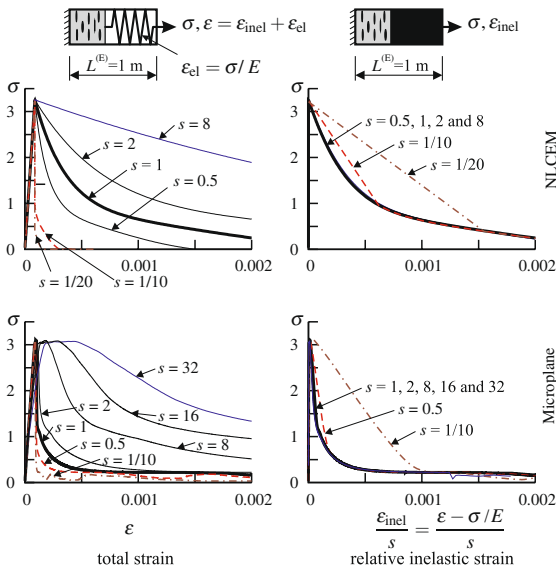


Fig. 3 Effect of varying: fracture energy G_F in NLCEM model (top); and crack band width c_b in M4 model (bottom) in a single finite element under tension. Left: stress vs total strain curves; Right: stress vs scaled inelastic (fracturing) strain

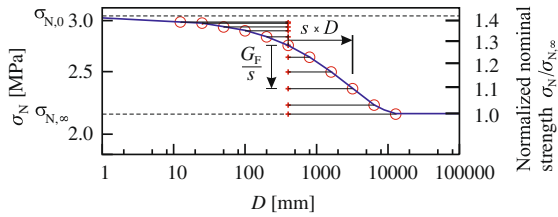


Fig. 4 Strength scaling using varying fracture energy G_F (or c_b) in a logarithmic size effect plot

situation is more complicated when randomizing the tensile strength and material toughness simultaneously.

3.3 Three-dimensional modeling

We have mentioned that the two dimensional models were created assuming plane stress conditions. One might get an impression that this simplification could be a source of an error, because the smallest specimen width is not negligible compared to other dimensions, see Fig. 1 left. Also, one can argue that a 2D model can be insufficient, because in the experiment, the hinges (pendulum system) could freely rotate in all directions enabling also out of plane rotation.

We have modeled the dog-bone specimens of all sizes in the three dimensional version of ATENA program using the same material law (fracture-plastic model NLCEM). The study was performed (i) with uniform stiffness distribution and also (ii) with a three-layer material of three different Young's moduli E .

In the homogeneous case we have used the same elastic modulus as in the two-dimensional models. There is nearly no difference between the 2-D and 3-D model responses. The maximum forces and the σ - ε diagrams are almost identical, see Fig. 5. The only marginal difference observed with small specimens was that the strains obtained in the core of the neck cross section was slightly greater than the strains obtained in the front and back surfaces. This might be a result of inducing tension in point hinges placed in the bottom and top loading platens that were not infinitely stiff. The reason for using the point hinges was to allow rotations of the platens in all directions. The diagrams of the medium sized and large specimens did not differ in the pre-peak branches, see Fig. 5. Large specimens in 3D showed different shapes of the post-peak branches obtained in the front and back faces. The

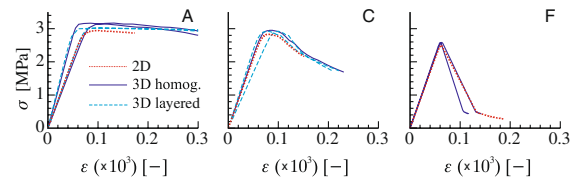


Fig. 5 Comparison of σ - ε diagrams obtained with 2D and 3D models

reason is that numerically the symmetry of the model was lost and the specimen started to flex at the onset of strain localization.

As for the nonhomogeneous case we have used the values and followed the concept of a previous study by van Vliet and van Mier (1999). It has been speculated also by Vořechovský (2007) that the effect of out-of-plane flexure might be an additional reason for average strength drop noticeable with small specimens. One might expect that in the smallest specimens the crack front is not initiated over the whole specimen width. Rather, due to stiffness inhomogeneity induced by the casting procedure (causing, in fact, internal eccentricity) the crack might initiate from the front face and the specimen flex out of the 2-D modeling plane. The authors of experiments have reported that due to the casting of the specimens, the front layers have different material properties than the back layers. Van Vliet and van Mier (1999) have shown that the nominal strength drop for the smallest size can nearly entirely be explained by strain/stress gradients that can develop due to the specimen's shape, eccentricity of the external load, material inhomogeneity and eigen-stresses due to differential shrinkage. They performed a thorough study using a linear model in which they considered normal stresses due to (i) tension (with a stress concentration factor corresponding to the dog-bone shape), (ii) bending moment due to the in-plane eccentricity and (iii) the out-of-plane bending moment caused by different stiffness in the casting and mould sides. They showed that most of the observed size effect could be explained with such a model.

We have modified the homogeneous 3D model by dividing the width of 100 mm into three layers of different thicknesses depending on the manufacturing process (see Fig. 6 right). The weighted average of the three moduli was equal to the modulus used in the homogeneous case. The three values 35.13, 30.59 and 24.93 GPa were set such that their ratios are equal to the ratios used by van Vliet and van Mier (1999). Their

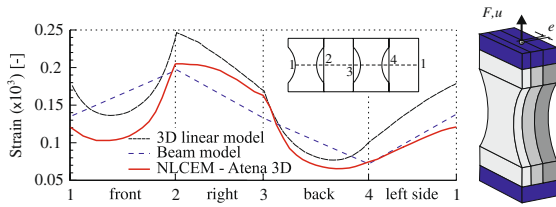


Fig. 6 Left: Strain distribution along the edges of the smallest cross section of an eccentrically loaded inhomogeneous specimen. Comparison of our ATENA results with analyses by van Vliet and van Mier (1999). Right: Three-layered inhomogeneous model in ATENA 3D software

reasoning was as follows: the front face is less stiff and this causes an internal eccentricity. Therefore, micro-cracking starts to initiate from the front face leading to a further decrease of local stiffness and increasing the micro-cracking even more. However, our computations with three dimensional models employing nonlinear material law did not support this idea. For large sizes the layered material stiffness makes no difference due to negligible specimen width compared to other dimensions. In small size specimens the response is relatively ductile, see Figs. 2 and 5. Even though the cracking did initiate from the front surface rather than from the back surface (see Fig. 1a) the inelastic response of material points is nearly perfectly elastic-plastic and the overall behavior is also ideally elastic-plastic.

The greatest difference predicted by the models was obtained with medium sized specimens C where the response is between the brittle and plastic limits and the 100 mm width is still comparable to other specimens dimensions. For specimen size C we present the computed strain profile in the linear pre-peak phase along the edges of the smallest cross-section (neck). Figure 6 compares these computations with previously obtained results of van Vliet and van Mier (1999). These computations confirm that the strain is far from uniformly distributed over the cross section and microcracking does not initiate simultaneously (even if the material was homogeneous). This fact supports the conclusion of van Vliet and van Mier (1999) that the nominal strength σ_N increases from A to C and then decreases as the size goes to F and that this can be partly explained by the effect of strain gradients. On the other hand, when the effect of nonlinear material response is taken into account, one must consider that strain gradients obtained in linear analysis do not hold in fully micro-cracked small specimens. Fig. 17 in (van Vliet and van

Mier 1999) shows that linear analysis with strain gradients qualitatively overestimates the strength drop of small specimens. Our linear elastic strain profile presented in Fig. 6 has slightly less peaking thus suggesting that there is a strong sensitivity of the peak strain on the way the stiffness is distributed. The conclusion is that possible strength drop obtained with the smallest specimens might still be explained partly by a strong non-homogeneity (presence of aggregates—grains up to 8 mm size) combined with out-of-plane eccentricity due to casting procedure, but the homogeneous model based on cohesive stresses (perfectly plastic glue in the limit) is not able to reproduce it.

Another possible cause was described and numerically studied in the preceding paper by Vořechovský (2007). The hypothesis was that the smallest specimen suffers the most from having a surface layer of a material with lower stiffness and strength. This can explain the strength decrease in small specimens. A parametric study with varied layer thickness and material strength reduction in that layer is presented in that paper, Sect. 4. The deterministic size effect studied until this point was automatically included in the weak layer computation because the same material model and parameters were used. However, the most important effect of strength reduction for large specimens cannot be modeled by deterministic effects studied so far. Neither is the model able to represent the strength scatter because randomness has not been considered in the model yet. Section 4 is focused on modeling local material strength parameters as a random property. Before proceeding to those results, it is important to see how variations in f_t of NLCEM model [K1 in microplane model] influences the response of a single finite element.

3.4 Effect of varied f_t and K1 at a finite element level

Let us now study what happens if f_t is randomized only in NLCEM model of one finite element under uniaxial tension. Figure 7 right studies such a situation, where we have multiplied the original tensile strength by $s = 1/2, 1$ and 2 . Since the fracture energy is not scaled, the initial softening slope of σ – ε diagram depends on the peak stress f_t to keep the same area under the curve. We can write that if $f_t \propto s$ then $G_F = \text{const}$. Therefore, if $s > 1$ the same element becomes stronger but ‘more brittle’ and dissipates the original amount of energy. The initial softening slope

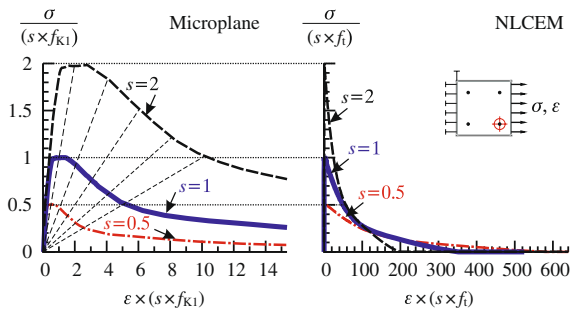


Fig. 7 Effect of varying strength $K1 [f_t]$ in microplane (left) [NLCEM (right)] models, respectively, on uniaxial tensile response of a single finite element

is in perfect negative dependence on f_t , while G_F is independent of f_t . Therefore, the size effect curve of the whole structure in Fig. 2 bottom right (or Fig. 4) computed with NLCEM model cannot be just moved up and down by changing f_t only (G_F is not proportional to f_t). One would have to multiply G_F by s^2 to achieve it because the characteristic length $\ell_{ch} \propto s^{-2}$.

A somewhat different situation is when strength parameter $K1$ is varied in the microplane model. Fig. 7 left shows results when a single element has $K1$ multiplied by $s = 1/2, 1$ and 2 . The tensile strength of one element scales linearly with s , but the whole $\sigma-\varepsilon$ is scaled radially, keeping the instantaneous softening slopes equal at corresponding loading stages. In other words, if $f_t \propto s$ then $G_F \propto s^2$ and the characteristic length $\ell_{ch} = \text{const}$. This can be viewed as a perfect positive dependence between f_t and G_F .

Note that, there can be imagined another alternative in which, with $f_t \propto s$ the energy $G_F \propto s$. The softening curve would have to decrease towards an identical strain value irrespective the peak stress f_t . The characteristic length $\ell_{ch} \propto s^{-1}$. This would also imply a perfect positive dependence between f_t and G_F .

These illustrations are important when randomizing both peak stress and fracture energy simultaneously. The most frequent combination in academic studies is the simultaneous randomization of G_F and tensile strength f_t . For example, it was shown previously by Vořechovský (2004b), Vořechovský and Novák (2004) that a strong positive correlation between these two parameters, when they are both randomly varying spatially, increases the slope of size effect curve in the transitional region between the two asymptotic limits (positive correlation, in fact, speeds up the convergence towards the classical Weibull statistical size effect).

4 The stochastic model

We believe that the strong size effect on strength in the experimental data is predominantly caused by the spatial variability/randomness of local material strength. Therefore, in the previous study (Vořechovský 2007), we considered the strength related parameter in the microplane model denoted $K1$ in ATENA to be random, and performed Monte Carlo type simulations for each size of specimen. The same strategy was performed here also with the NLCEM fracture-plastic material model in which we randomized the tensile strength f_t . In particular, we sampled 64 random field realizations of the parameter $K1 [f_t]$ for each size and computed the responses (complete $\sigma-\Delta u$ diagrams, stress fields, crack patterns, etc.). The reason for sampling the local material strength by a random field instead of by independent random variables is that we believe that in reality the strength of any two close locations must be strongly related (correlated) and that such a relationship can be suitably modeled by an autocorrelated random field, see Fig. 8 right.

The distribution of local tensile strength at each material point is assumed to be identical and Weibull distributed, see Fig. 8 top-left. The reason for selecting Weibull distribution is that the strength of large sized structures obeys this form of extreme value distribution. It can be argued that small to medium structures have Gaussian strength distribution with Weibullian left tail (Bažant and Pang 2007). A simple argument to support such a distribution comes from the fact that a random

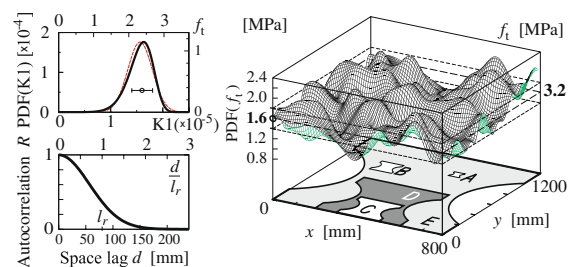


Fig. 8 Top-left: Weibull probability distribution function of the randomized parameters $K1 [f_t]$ (Eq. 5) compared to Gaussian distribution with equal mean and variance (dashed line). Bottom-left: Autocorrelation function (Eq. 6). Right: Realization of a Weibull random field of $K1$ compared with dog-bone specimens type A – E. The dashed lines correspond to the mean and mean \pm one standard deviation of $K1 [f_t]$

strength of Daniels's fiber bundle model has this form (see e.g. Vořechovský and Chudoba 2006, Bažant and Pang 2007 for more details on the distribution). More fundamental arguments are presented in another paper in this issue (Pang et al. 2009). However, the difference between the Gaussian and Weibullian core with equal mean value and variance (see Fig. 8) has a negligible effect on the first few statistical moments of a random strength of small to medium structures. More importantly, the strength of large structures depends solely on the Weibull left tail, which is modeled correctly when assuming the whole distribution Weibullian.

The local probability of failure p_f (cumulative Weibull distribution function F_σ) depending on stress level σ reads:

$$p_f = F_\sigma(\sigma) = 1 - \exp\left[-\left(\frac{\sigma}{\sigma_0}\right)^m\right] \quad (5)$$

where σ_0 = scale parameter of Weibull distribution, a value of $1.6621 \cdot 10^{-4}$ MPa is used for K1 and 3.4 MPa for f_t ; m = shape parameter of Weibull distribution (dimensionless, depends solely on cov = coefficient of variation), $m = 7.91$ being used for random K1 and f_t in the two parallel studies.

To obtain results consistent with the previous deterministic analyses, we kept the value of parameters f_t [K1] as the mean values, i.e. 3.2 MPa [$1.5644 \cdot 10^{-4}$]. The second parameter of Weibull distribution has been set with regard to the cov of the nominal strength of the smallest specimen A (in experiments the cov of strengths of size A was 0.16). This choice is supported by the fact that size A has the largest sample size (10 replications, see Table 1). Therefore, the estimation of variance has a higher statistical significance than for other sizes. We will explain later on why this choice is not quite correct. For simplicity, we used the value of $\text{cov} = 0.15$ (15% variability of local material strength). This is a relatively high value implying the unusually low Weibull modulus mentioned above. Note that a different choice of Weibull modulus based e.g. on the scatter of nominal strengths for size C would lead to a greater m (≈ 16 , see the rightmost column of Table 1) and therefore less scattered results ($\text{cov} \approx 0.08$) and a milder slope in the asymptotic size effect curve for $D \rightarrow \infty$. On the other hand, the scatter of experimentally obtained peak forces is much higher for size A suggesting that there was a strong influence of additional imperfections in shape, geometry and boundary

conditions (eccentricity, etc). As will be seen later, the asymptotic slope of the mean size effect $-2/7.91$ does not equal the value of $-2/12$ suggested by averages of all sizes except size A (and used in a simple Weibull slope fit by van Vliet and van Mier (2000a,b)). The issue of the correct choice of statistical scatter of the material strength is further discussed in Sect. 5.

A discretized random field can be viewed as a set of (auto)correlated random variables. The most important parameter (in a given form of autocorrelation function) is the autocorrelation length controlling the distance over which the random material strengths are correlated. We used the squared exponential autocorrelation function (Fig. 8 bottom-left):

$$R = \exp\left[-\left(\frac{d}{l_r}\right)^2\right] \quad (6)$$

where d = distance between two points; l_r = correlation length, a value of 80 mm used for a random fields of K1 [f_t].

The correlation length l_r is here assumed to be a material (and possibly structural) constant related to both the microstructure (grain size and defect distribution and their frequency, i.e. on their distance from each other), and also on the production technique (compacting, etc.). The autocorrelation function takes values close to unity for any two close points in the specimen (unit correlation is the upper limit for two coinciding points). For a pair of remote points the autocorrelation decays to zero implying no statistical correlation for the material properties of those two points. It can be shown that for specimens much smaller than one autocorrelation length, the realization of a random field of the local strength K1 is a constant function over the whole region (see Figs. 8 right and 9), and all local strengths of the whole specimen can be represented by just one random variable (instead of a number of spatially correlated variables). Since the specimen's nominal strength is just a simple transformation of the input strength parameter K1 [f_t] (no spatial variability, allowing cracks to localize in other locations than in deterministic analysis), we knew that the mean nominal strength of the smallest specimen will be the same as that obtained by deterministic analysis. That is why we used the K1 [f_t] from deterministic analysis as the mean value of the random field of K1 [f_t]. We set the correlation length l_r such that the computed size effect curve 'bends' between a constant and Weibull

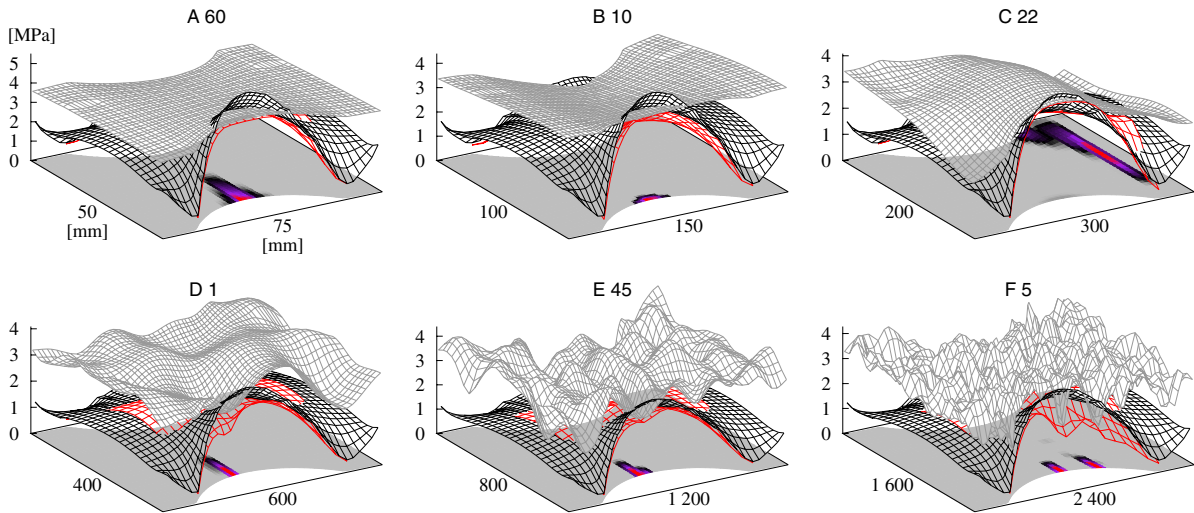


Fig. 9 Stress/strength fields corresponding to the peak load for selected realizations and specimen sizes. Results are computed with randomized NLCEM material model. Fields from top: random strength field (threshold), principal stress of a brittle material

scaled to correspond to the peak load (nominal strength), actual principal stress at peak load, cracking strain at the bottom plane. See also selected realizations in Fig. 10

asymptotes at a crossover specimen size C , which better fits the experiments, see also Sect. 4.1.

The samples of random fields evaluated at the locations of integration points were simulated by methods described in Vořechovský (2008, 2004b). In the method, the support of the field is discretized (nodes of the random field mesh may coincide directly with the integration points of the FEM mesh). Based on the discretization and a given autocorrelation function (Eq. 6) an autocorrelation matrix C is assembled. Such a matrix is symmetric and positive definite and has orthogonal eigenvectors Φ and associated eigenvalues Λ such that $C = \Phi \Lambda \Phi^T$. The (discretized) Gaussian random field X is expanded using a Gaussian random vector ξ and the computed eigenmodes as $X = \Phi (\Lambda)^{1/2} \xi$. If non-Gaussian fields are to be simulated, the Nataf model is usually employed (Liu and Der Kiureghian 1986). The simulated random fields are stationary, isotropic and homogeneous. Briefly, the described orthogonal transformation of the covariance matrix has been used in combination with Latin Hypercube Sampling of the random part of field expansion (Novák et al. 2000). Such a combination proved itself to be very effective in providing samples of random fields leading to high accuracy in estimated response statistics compared to classical Monte Carlo sampling. Numerical studies documenting this efficiency are published

in (Vořechovský 2008). This is an extremely important property in cases when the evaluation of each response is very time consuming. In our case the evaluation is represented by one computation of response by the non-linear finite element method with the microplane or NLCEM material model inside. Obviously, this is very expensive and we must keep the number of simulations as low as possible. The number of 64 simulations was tested to be high enough and to provide stable and accurate statistical estimates of fields' statistics (averages, sample standard deviations, autocorrelation structure) as well as reproducible estimates of structural response statistics (nominal strength etc.).

The automatic simulation of all structural responses was done by SARA software integrating (i) ATENA software (evaluation of response) and (ii) FREET software (Vořechovský 2004b, Novák et al. 2003b, 2006) (simulation of samples of random parameters, statistical assessment).

In Fig. 10 we plot selected realizations of the random strength field in NLCEM model for all sizes A – F, some of which are better visualized in Fig. 9. Similarly, Fig. 11 presents selected plots for randomized microplane model. We note that a similar scaling rule as in Eq. 2 can be written for the role of statistical length (here in the form of autocorrelation length l_r). For a given random strength field (statistical distribution and

Fig. 10 Simulated random strength field realizations and corresponding crack patterns in deformed specimens right after attaining the maximum force F_{max} . Fields were simulated and crack widths were computed at the integration points of finite elements using the NLCEM material model

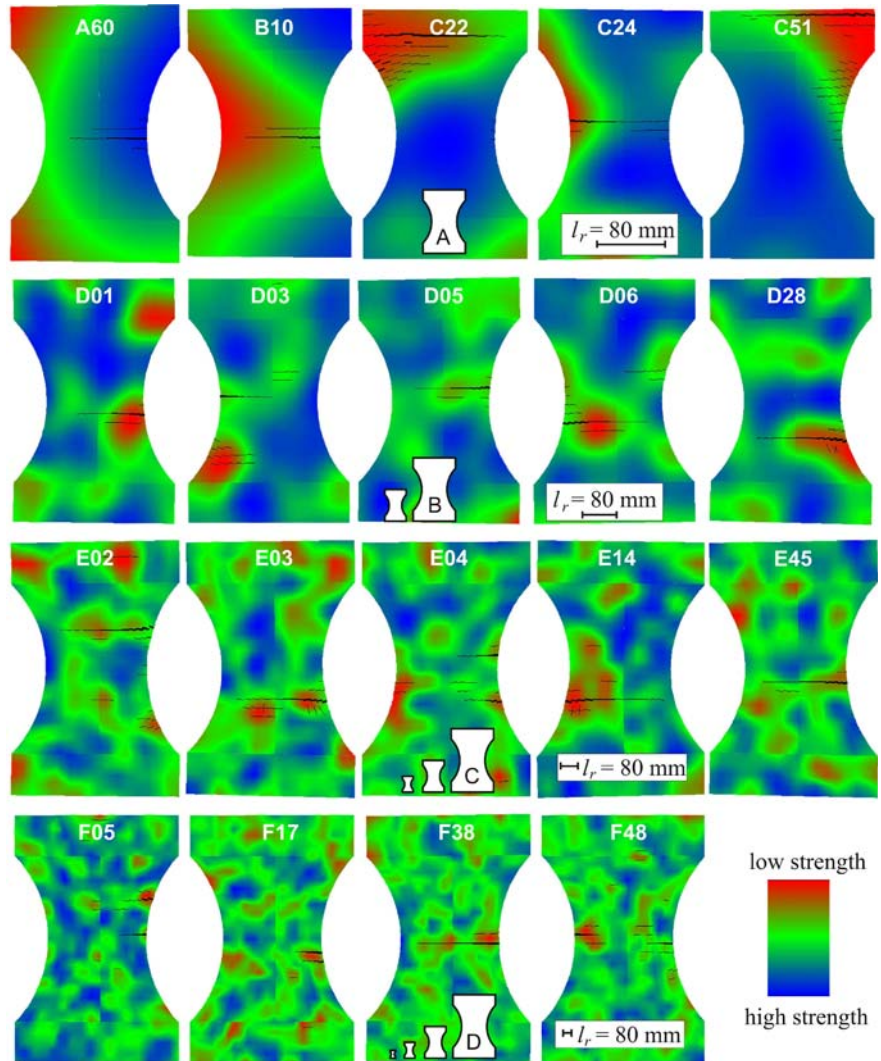
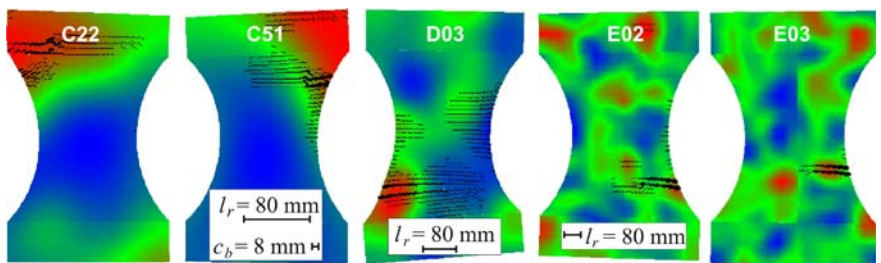


Fig. 11 Selected crack patterns from the series with randomized microplane models. Intended for direct comparison with Fig. 10



autocorrelation structure) only the dimensionless proportion D/l_r matters (recall the dimensional analysis):

$$\text{for } \forall s > 0 : \sigma_N(D, l_r) = \sigma_N(sD, s l_r) \quad (7)$$

Again, this can be used to simplify modeling because one size can be used with varying l_r instead of varying D with a constant l_r . Similarly to Eq. 2, this property

illustrates the scaling properties with l_r standing for a *probabilistic (or statistical) scaling length*. Similarly as with the deterministic size effect caused by stress redistribution in FPZ, the probabilistic size effect curve represents a transition between two asymptotes (horizontal for $D \rightarrow 0$ and an inclined straight line for $D \rightarrow \infty$). The transition happens around a cross-over size l_s

(discussed below in Sect. 4.1), i.e. when the non-dimensional size D/l_s takes values approximately between 0.1 and 10.

It can be seen that as the ratio of autocorrelation length and specimen size D decreases, the rate of spatial fluctuation of random field realizations grows. Therefore, there are an increasing number of locations with low material strength (locations prone to failure). Or, in other words, with increasing specimen size there is an increased probability that there will be a weak spot in highly stressed regions. This effect has long been referred to as the statistical size effect. The classical statistical size effect is modeled by the simple weakest link model and is usually approximated by the Weibull power law (Weibull 1939). However, as explained in (Vořechovský 2004b,a, Vořechovský and Chudoba 2006), the classical Weibull model is not able to account for spatial correlation between local material strengths. Rather, the Weibull model is based on IID (independent and identically distributed) random variables linked in series. The effect of such a consideration is that the strength of an infinitely small specimen is infinite. In the Weibull model every structure is equivalent to a chain under uniaxial tension, a chain of independent members having an identical statistical distribution of stress. If the local strength is modeled by an autocorrelated random field (and we consider the autocorrelation length to be a material property), the small size asymptote of strength is equivalent to the distribution of local material strength. On the other hand, the large size asymptote is exactly identical to that of the Weibull model (for a proper choice of reference length and the corresponding scale parameter of Weibull distribution in the Weibull model). The autocorrelation length plays an important role as a statistical scaling length in a material controlling the transition from a one strength random variable model (full correlation in small structures) to many independent local strengths (large structures, Weibull model); see (Vořechovský 2004b) for details.

In Fig. 12 we plot computed sets of ‘nominal stress–strain’ (σ – ε) diagrams obtained with the NLCEM model and sketch the definition of strain (the separation of two measuring points Δu over the control length). The corresponding diagrams obtained with microplane law were published in (Vořechovský 2007). In there, several selected load displacement curves were highlighted and the corresponding realizations of random strength fields of microplane K1 parameter together

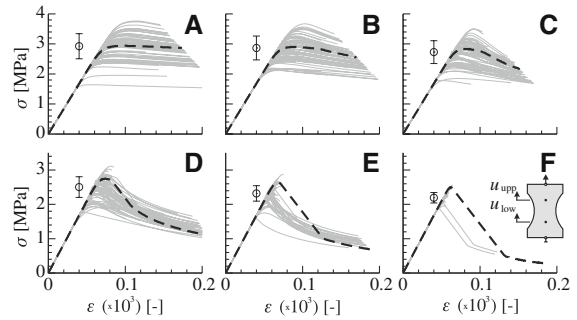


Fig. 12 Nominal stress-strain diagrams (64 realizations) obtained with randomized NLCEM material model

with crack patterns were presented. In the same paper, besides the most frequent simple σ – Δu functions, we have purposely highlighted several curves with unusual shapes (snap-back type or ‘a loop’). When testing concrete structures in routine practice such special shapes can only occasionally be experimentally measured. They would indicate that the control length was not properly designed (with respect to the specimen shape and material strength variability) and that localized strains occur outside the control length. As discussed there, some of the unusual or unexpected curves were obtained partly due to the definition of displacement Δu , and mainly due to the spatial randomness with (too) high variability. In the analyses with NLCEM material law, these loops nearly did not occur. For comparison purposes of the peak strength of the deterministic σ – ε diagrams with the mean values of nominal strength are added into Fig. 12. The difference between them grows with specimen size. While for size C the mean strength still nearly coincides with the peak of the deterministic diagram, for specimen size F the deterministic curve is above all 64 random realizations of the diagram, see Fig. 12. This feature is related to the transition from the *central limit theorem* applicable to small sizes (nominal strength is a result of a sum of random strength of many links arranged in parallel) to *extremes* of independent variables (the smallest local strength compared to stress dictate the structural strength).

The crack patterns of two randomly chosen specimens A 60 and B 10 (see Fig. 10) show the most frequent location of strain localization. Fig. 9 shows how the maximum principal stress field would look at the peak load if no redistribution takes place and when the stress could exceed the local strength. This figure also shows the actual (redistributed) stress field that

can be described as a ‘deformable ball pressed towards sealing (strength realization) from bottom’. Samples of random fields in both cases (A, B) are nearly constant functions and therefore there is no space left for the weakest link principle. The small eccentricity of load and relatively narrow neck of dog bone specimens guarantee that cracking will initiate on the right side of the neck. Pattern C 22 in the same figure documents that the local strength can be, in some locations, so small that the relatively low stresses in that location can initiate fracturing. In specimen C 22 the rotation of platens was opposite to the usual direction. Since the damage localized out of the distance (control length) over which we measured the separation Δu , the corresponding σ - ε has the snap-back-like shape. The fact that the specimen breaks in the relatively low stressed region is associated with the relatively high variability of local material strength. Simply, the realization of the strength field in the cracked region was the closest to the principal tensile stress profile, see Fig. 9. If a different strength distribution was chosen (especially lower variability), the occurrence of fracturing outside the neck area would be suppressed. The selection of material parameter variability was in this numerical example too high as will be discussed in Sect. 5. Pattern C 51 is also quite unusual. Similar features can occasionally be found in series D. We illustrate the random sampling of crack initiation in the same figure. In series F the autocorrelation length becomes so small compared to specimen dimension that again cracks mostly initiate on the right side of the neck in nearly all cases, see Fig. 9. The specimen F 5 in Fig. 9 illustrates the case when the strength realization is hit by the stress field at two points simultaneously. In such cases, two major parallel cracks can develop at the peak load even in a relatively large structure with small amount of stress redistribution prior reaching the peak load.

In series A, we never reported a snap-back-like curve due to cracking outside the measuring distance, because the random field is nearly a constant function over the specimen. We can conclude that the most interesting processes happen in specimens with a dimension comparable to one or two correlation lengths (region of transition from one random strength variable to a set of independent strength variables).

From comparisons in Sect. 3.4 it transpires that comparisons between results with randomized f_t in

NLCEM and K1 in microplane models cannot be done directly. Rather, it was expected to shed some light on the effect of having a perfect positive dependence between material peak stress and fracture energy. It can be seen that the post-peak curves in the bundles of diagrams in Fig. 12 computed with NLCEM are steeper when they reach a higher peak (and opposite). On the contrary, the softening slopes of diagrams in each bundle obtained with the microplane model (Fig. 4 in (Vořechovský 2007)) have the same post-peak slope, if the snap back did not occur.

A question appears: which of the three alternatives for randomization of tensile strength, fracture energy and characteristic length described in Sect. 3.4 is more realistic for real concrete? We do not give an answer, because the two compared material models behave differently clouding the picture. One would have to perform simulations with a single material model in which the parameters are varied simultaneously according to the three alternatives.

It might be interesting to compare the crack patterns obtained with microplane model and NLCEM model when the realization of a random field of K1 [f_t] is identical (one is just a multiple of the other). We have selected five crack patterns from our previous study (Vořechovský 2007) and plot them here for comparison. An interested reader can find the same size and number in Figs. 10 and 11. One can see that NLCEM model predicts much more localized cracks compared to the microplane model. In D03, for example, microplane model predicts quite diffused cracking far from the neck while NLCEM model just predicts some microcracking there and the final magistral crack passes through the neck. The relatively diffused cracking predicted by microplane model corresponds to milder slopes of the pre-peak branches of diagrams in Fig. 2. We note that the first guess might be different: when a weak element starts to soften in NLCEM, it is an element with a milder softening slope. This would support somewhat tougher behavior of NLCEM models which is not found here.

Finally we note that, in contrast to the experiments, we did not control loading by displacement increments Δu . Instead, we loaded the specimens by displacement at the ends, and therefore we were able to monitor the snap-back type of curves without any difficulty.

4.1 The Weibull integral, extremes of random fields, reference and representative volumes

We were able to simulate the random responses of specimens smaller than A with random fields of K1, and moreover we could simply use random variable sampling to represent randomness in the small specimens (each realization becomes a random constant function over the specimen). On the other hand, it becomes very expensive to simulate samples of random fields of specimens much larger than F due to the need of a dense discretization. Approaches already exist to overcome the computational difficulties with the stochastic finite element computation of large structures (Vořechovský et al. 2006) but we will present another technique here. Fortunately, only strength is random in our analysis and we can use the classical Weibull integral for large structures. As explained in (Vořechovský 2004b,a, Vořechovský and Chudoba 2006), if the structure is sufficiently large, the spatial correlation of local strengths becomes unimportant and the Weibull integral yields a solution equivalent to a full stochastic finite element simulation. We will briefly sketch the computational procedure of evaluating the Weibull integral for structural failure probability: details can be found e.g. in (Bažant and Planas 1998). The Weibull integral has the form:

$$-\ln(1 - P_f) = \int_V c[\sigma(\mathbf{x}); m, \sigma_0] dV(\mathbf{x}) \tag{8}$$

where P_f = probability (the cumulative probability density) of failure load of the structure; $c[\bullet]$ = stress concentration function.

There are several possible definitions of the stress concentration function, see Bažant and Planas (1998). In the studied specimens the major contributor to the stress tensor is the normal stress σ_{yy} . The field of stress σ_{yy} nearly coincides with the principal tension σ_I . Since only tensile stresses are assumed to cause a failure, we defined the stress concentration function simply as:

$$c[\sigma(\mathbf{x}); m, \sigma_0] = \frac{1}{V_0} \left\langle \frac{\sigma_I(\mathbf{x})}{\sigma_0} \right\rangle^m \tag{9}$$

where $V_0 = l_0^n$ = reference volume associated with m and σ_0 .

In Fig. 1b, we plot the computed field of the maximum principal stress (tension) over a specimen in an elastic stress state. Numerical integration of this stress field for different specimen sizes and failure probabilities can be suitably rewritten in dimensionless coordinates so that the computation becomes extremely easy.

In particular, let $\xi = \mathbf{x}/D$, consider unit thickness b and set the maximum elastic principal stress field $\sigma_I(\mathbf{x}) = \sigma_N \mathbf{S}(\xi)$ where σ_N is the nominal stress and $\mathbf{S}(\xi)$ the dimensionless stress distribution independent of D . If, in accordance with Bažant et al. (2007a), we substitute these and $dV(\mathbf{x}) = D^n dV(\xi)$ into Eq. 8, we get $-\ln(1 - P_f) = (\sigma_N/\sigma_0)^m N_{eq}$ or

$$P_f(\sigma_N) = 1 - \exp \left[-N_{eq} \left(\frac{\sigma_N}{\sigma_0} \right)^m \right] \tag{10}$$

where the equivalent number of identical links in a chain

$$N_{eq} = \left(\frac{D}{l_0} \right)^n \Psi \tag{11}$$

depends on a geometry parameter

$$\Psi = \int_V S^m(\xi) dV(\xi) \tag{12}$$

This geometry parameter characterizes the dimensional stress field that depends only on the structure geometry and boundary conditions. As defined in a recent work by Bažant et al. (2007a), N_{eq} can be interpreted as the equivalent number of equally stressed material elements of a size for which the reference material statistical properties has been measured. At this place, we mention that asymptotically, the structure becomes a chain of N_{eq} equally stressed RVEs in a series, see Fig. 13 right. Note that the number of the chain elements with a random strength is proportional to the scaling dimension n (two in our case). It is an occasional practise to place a fiber bundle model (FBM) inside a region in which the crack is expected to be propagating, see Fig. 13. Note however, that for the purpose of asymptotic strength prediction, this approach is inadequate. It

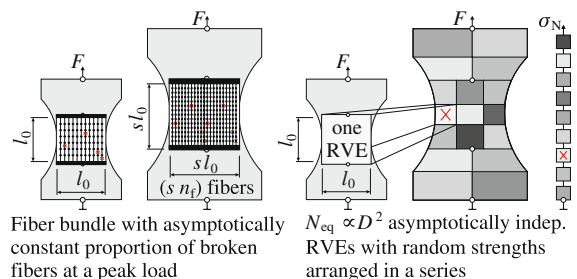


Fig. 13 Illustration of a random strength representation. Reference size and s -times scaled structure. Left: incorrect scaling of strength using FBM. Right: concept of RVEs in a solution using Weibull integral

is known that increasing the number of parallel fibers n_f (or microbonds) in the FBM asymptotically does not decrease the mean strength per fiber (although the variance decreases inversely proportionally to n_f , see e.g. Vořechovský and Chudoba 2006). So, scaling the structure size s times brings about only length effect, which is a one-dimensional effect, not two-dimensional effect as it should be ($N_{eq} \propto D^2$). The prediction of an asymptotic random strength distribution would than be incorrect, see (Vořechovský and Chudoba 2006) for more details.

The present derivation is fully complying with the recent work by Bažant et al. (2007a) in which the representative volume element (RVE) is defined as the smallest material volume whose failure causes the failure of the whole structure (this definition is valid for positive geometry structures, i.e. structures that fail, under load control, as soon as the first RVE fails). The concept of equivalent number N_{eq} of equally stressed RVEs is introduced to simplify the problem in cases when the stress state is not uniform and the actual number identical volume elements are subjected to different stresses. In both cases, the probabilities of failure of the structure P_f are identical.

Consider now a case when all the RVEs are *independent* of each other (as is the case of asymptotically large structures). Since the structure survives as a whole if and only if all the RVEs survive, one can write the survival probability as a product $1 - P_f = (1 - P_1)^{N_{eq}}$ or, equivalently (Bažant and Pang 2007):

$$P_f(\sigma_N) = 1 - [1 - P_1(\sigma_N)]^{N_{eq}} \tag{13}$$

This failure probability tend to

$$\lim_{N_{eq} \rightarrow \infty} P_f(\sigma_N) = 1 - \exp[-N_{eq} P_1(\sigma_N)] \tag{14}$$

where $P_1(\sigma_N)$ is the cumulative distribution function of the strength of one RVE. Clearly, as $N_{eq} \rightarrow \infty$, the structural strength distribution converges to Weibull form.

Using Eq. 10 we can easily relate the parameters of a random *material strength* to the mean value of the *structural strength*:

$$\overline{\sigma_N} = \frac{\sigma_0}{N_{eq}^{1/m}} \Gamma(1 + 1/m) = \frac{\mu_0}{N_{eq}^{1/m}} \tag{15}$$

where $\Gamma(\cdot)$ is the Gamma function. The material strength is represented by the parameters of a random RVE strength considered to follow Weibull distribution or a Gaussian distribution with a Weibull tail described

by the shape parameter m and corresponding scale parameter σ_0 , a pair yielding the mean strength value μ_0 of one RVE of size l_0 .

In the particular case of studied dog-bone specimens, the Weibull solution gives the following results. First, the thickness $b = 100$ mm is not scaled and therefore it does not contribute to the strength scaling. Therefore we ignore the thickness and define volumes as areas. When $m = 7.91$, as studied before, the geometry parameter defined in Eq. 12 can be computed to equal $\Psi \approx 0.574$. If one selects the length l_0 to equal the autocorrelation length $l_r = 0.08$ m (see below for reasons), each RVE has the mean strength $\mu_0 = 3.2$ MPa and scale parameter $\sigma_0 = 3.4$ MPa. The number of equivalent RVEs in specimens of various sizes can be calculated using Eq. 11, for size F the formula gives $N_{eq} \approx 230$. Therefore, the average nominal strength of size F is approximately 1.61 MPa. The resulting mean size effect for other sizes is plotted in Fig. 14 (asymptotic mean size effect curve). Let us also mention that another way of simulating the random strength of large structures can be done utilizing the stability postulate of extreme values (Fisher and Tippett 1928). Such a computational procedure is an elegant trick using the recursive property of the distribution function and is described in Bažant et al. (2007b), Novák et al. (2003a), Vořechovský (2004b) together with applications. The results of such an approach (and also the Weibull integral as presented here) are valid only for extremely large sizes where the effects of structural nonlinearity (causing stress redistribution) disappear. There is no characteristic material length in the classical (local) Weibull theory, because the Weibull size effect is self-similar—a power law with no characteristic length and no upper bound. Rather, l_r (or V_0) in Weibull theory is simply a chosen unit of measurement to which the spatial density of failure probability is referred. For small sizes there are two problems: (i) the spatial correlation of local strengths and (ii) the effect of stress redistribution. The result of the Weibull integral must be a straight line in a double logarithmic plot of size versus strength (the size effect plot is a power law). These two issues will be discussed next. Note that there exist also a nonlocal alternative to the Weibull integral that is commented on and compared with the classical local Weibull integral in Sect. 5.2 of (Vořechovský 2007).

Because the statistical and energetic physical causes of size effect are different and independent, the statistical length l_r cannot be affected by changes in the

deterministic length c_b (or similarly changes in G_F). The mean value of a random nominal strength σ_N must be bounded when $D \rightarrow 0$, (i.e., the statistical size effect cannot cause a strength increase when the structure is too small as in the classical Weibull theory). The upper bound on the mean statistical size effect can be easily calculated as the deterministic strength of a structure with no stress redistribution allowed ($c_b/D \rightarrow 0$ or $G_F/D \rightarrow 0$), see the bottom horizontal asymptote in Fig. 14. The same bound is also obtained as the mean value of the distribution of extremes (minima) of random fields representing local material strength (Vořechovský 2004b, Vořechovský and Chudoba 2006).

To study the statistical size effect of structures with no redistribution, one has to select the size of the RVE in the case when a random material strength is described by random fields. Note that in the case of uncorrelated Weibull strengths the choice is arbitrary; the reference length is related to the strength scale parameter through a power law. In the autocorrelated case the choice depends on the autocorrelation length — the length l_0 must be equal to a length over which the local strengths are nearly uncorrelated. Therefore, we consider the equality between the autocorrelation length (Eq. 6) and the length l_0 from here on:

$$l_r = l_0 \tag{16}$$

An area $A_0 = l_0^2$ or a volume $V_0 = l_0^3$ has now the mean strength of μ_0 .

To show the difference between the statistical size effect in the Weibull sense and when autocorrelated strength is assumed, one must isolate the statistical effects from the deterministic effects. The pure statistical size effect (i.e. the size effect of the structure with no stress redistribution) can be numerically simulated by replacing the crack band or fracture energy with zero and using the same realizations of a random strength fields. Numerical results are plotted in Fig. 14 using a line with solid boxes and errorbars. One can see that the calculated mean size effect curve is a smooth transition between two asymptotic cases: the constant upper bound for small sizes and the Weibull asymptote for large sizes. The cross-over size l_s can be calculated from the equality of deterministic strength of a large structure $\sigma_{N,\infty} \equiv \sigma_N^{\text{det}}(\infty, c_b) \equiv \sigma_N^{\text{det}}(D, 0) = 2.15 \text{ MPa}$ and the mean Weibull strength of 3.2 MPa in Eq. 15. This equality yields

$$l_s = l_0 \Psi^{-1/n} \left[\frac{\mu_0}{\sigma_{N,\infty}} \right]^{m/n} \tag{17}$$

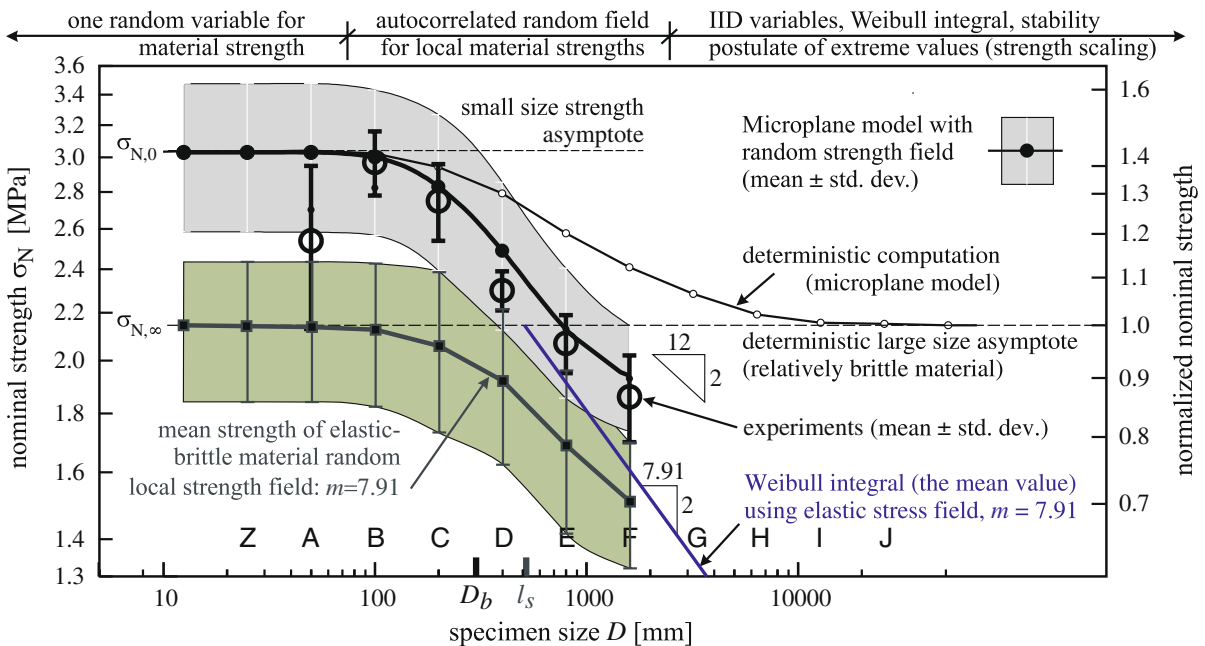


Fig. 14 Comparison of results in a size effect plot

which gives, in our numerical example $l_s \approx 510$ mm, see the abscissa scale in Fig. 14. The transition can be approximated using the formulas proposed earlier by Vořechovský (2004b), Vořechovský and Chudoba (2006) as approximations to extremes of random processes:

$$\overline{\sigma_N}(D) = \sigma_{N,\infty} \left(\frac{D}{l_s} + \frac{l_s}{l_s + D} \right)^{-n/m} \quad (18)$$

or

$$\overline{\sigma_N}(D) = \sigma_{N,\infty} \left(\frac{l_s}{l_s + D} \right)^{n/m} \quad (19)$$

The numerically obtained mean of statistical solution lies in between these two approximations. These formulas represent extension of extremes of stationary and ergodic Weibull random processes (Vořechovský 2004a,b, Vořechovský and Chudoba 2006) to n -dimensional random fields. The formulas were originally applied to predictions of the strength of thin fibers (Vořechovský and Chudoba 2006) and later in the context of the energetic-statistical size effect in quasi-brittle structures failing after crack initiation, see (Vořechovský et al. 2005, Bažant et al. 2007b).

5 Analysis of the results

By introducing three different scaling lengths we are able to independently incorporate three different effects in the model resulting in three size effects on nominal strength. The crack band width c_b (deterministic scaling length, linearly related to the fracture energy G_F) controls at which size the transition from ductile to elastic-brittle microplane model behavior takes place, and therefore it controls the transition between two horizontal asymptotes in the size effect plot (see Fig. 2 bottom right). The second introduced length (weak boundary thickness t_w) together with material strength reduction controls at which size there will be a significant reduction in nominal strength. The reduction becomes amplified with decreasing specimen size and causes an opposite slope of size effect than with the deterministic and statistical ones (see Fig. 2 of (Vořechovský 2007)). The last introduced length is the autocorrelation length l_r , controlling the transition from randomness caused by overall material strength scatter (one random variable for material strength) to a set of independent identically distributed random variables of local material strengths via an autocorrelated random

field. In other words, it controls the convergence to the Weibull statistical size effect based on the weakest link principle.

In the case of a random field description of local strength we can see the following behavior. If the possibility to redistribute stresses (nonlinear phenomena) is suppressed (vanishing characteristic length represented by c_b or G_F compared to specimen size), the Weibull asymptote is reached from bottom, see the solid boxes in Fig. 14. If the deterministic length is comparable to the statistical one, the transition to Weibull solution is from above, because small sizes exceed the nominal strength $\sigma_{N,\infty}$ (solid circles in the figure).

Numerical simulations show that the autocorrelation length may, with its role as a measure of the rate of fluctuation of local material parameters, significantly influence the damage process and the global response of the structure. Especially when *local strength* is varied randomly and the relative variability is high, the spread of damaged zones will be dependent on both: crack band size (or similarly nonlocal length in nonlocal damage models) and also on the autocorrelation length/structure. When the correlation length is much larger than the specimen, the realizations of a random strength are nearly constant functions and the damage spread is governed solely by the deterministic effects (stress fields and concentrations influenced by redistributions due to the nonzero nonlocal or crack band length), see A 60 in Fig. 9. Here, with reference to the discussion on the concepts of nonlocal averaging in Sect. 5.2 of (Vořechovský 2007), we note that the so-called fracture process zone size depends on actual stress fields, which are also influenced by presence of specimen boundaries, apart from the usually attached physical meaning of the function of the maximum aggregate size in concrete. All these can be put on the side of deterministic effects. On the contrary, when the spatial distance of serious local flaws or defects (the correlation length) is very small compared to the nonlocal length, the damage process will depend on interactions of zones in which the damaged material softens locally. The zones with a high local strength adjacent to the weaker zones act as ‘barriers’ for further spreading-out of damage, see e.g. F 5 in Fig. 9. Generally, the size of the damaged zone depends probably strongly (and nearly linearly) on the deterministic length and only weakly on the autocorrelation length of local strength field in our continuum model. If the autocorrelation length is smaller than the damage zone size in the deterministic case, it probably

slightly decreases the damaged zone size in the probabilistic case. Both lengths can be understood to rely on the same physical background—microstructural properties below the continuum level. However, a random spatial strength variability can also occur at the macroscopic level due to variable manufacturing process of concrete, etc.

The interplay of three independent material/structural lengths as sketched in this paper is very complicated. It would be nearly impossible to determine all these parameters from the available experimental data even if the model featuring the three effects was perfectly correct.

In Fig. 6 of (Vořechovský 2007), the estimated distribution function of nominal strength for all tested sizes as we obtained them from the full stochastic finite element analysis with are plotted. The discussion there explains that models of large specimens suffer from an insufficient discretization of the random field with respect to the autocorrelation length, see also F 5 in Fig. 9. This is a clear limitation of the random field approach. We sketch the size regions for different computational techniques used for the modeling of random strength above the plots in Fig. 14.

The resulting nominal strengths for all sizes obtained by nonlinear stochastic FEM are plotted and compared to experiments in Fig. 14. The figure is devoted mostly to microplane modeling because at this graph the NLCEM modeling yields comparable results (even if there were differences in the stress–strain curves and crack patterns and randomization of f_t and K_I are not directly comparable). We see that starting from size C the dependence of mean nominal strength on size is *predominantly statistical*, and we were not able to model it by deterministic model alone. We also included mean nominal strengths for sizes D, E, F and G obtained by Weibull integral.

The asymptotic slope of statistical size effect suggested by the trend of the means of the Weibull solution ($-n/m = -2/7.91$) is not in a good agreement with the scatter of measured nominal strengths for sizes greater than A. If we ignore the smallest size A where the variability of strength data is questionable, C is the size with most of replications (seven). Therefore, the standard deviation obtained from experiments is most significant for size C. The very last column in Table 1 presents the effective Weibull moduli computed from experimentally obtained averages and sample standard deviations. Mostly these m values are greater than that

of C meaning that the estimated scatter is less, which corresponds to the fact that there were less realizations (four or five only). The reason for A yielding much greater variability (and thus smaller effective m) must be explained by several other effects. Numerical simulations with a lattice model performed by van Vliet (2000) revealed that if a large grain is present in the surface layer of the specimen, the peak load can decrease considerably. Such a mechanism certainly contributes to the increased statistical scatter of nominal strengths in specimen type A. Even though the number of realizations for size A was ten, the information on scatter does not seem to be relevant. A better choice in this study would be $m \approx 14$ suggested mainly by the slope of the size effect curve for the two largest specimen sizes E, F. Note that the steeper slope at medium sizes C, D can be attributed to a combination of both deterministic and statistical effects.

The tendency of bundles of diagrams computed with NLCEM (Fig. 12) corresponds better with the experimental curves: the greater the size the steeper the post-peak slope. This was not true for the microplane models, see Fig. 4 of (Vořechovský 2007). With regard to the above mentioned comparison to randomization with a constant ℓ_{ch} (NLCEM) versus constant G_F (microplane), the comparison with experimental curves suggests that keeping the G_F constant is somewhat closer to reality than keeping a constant ℓ_{ch} .

We have also performed a study with NLCEM model in which we divided the fracture energy G_F by 16, thus shifting the deterministic transition to smaller specimens. In this way, the deterministic behavior previously obtained for size E becomes behavior of size A. The stress–strain diagrams then correspond much better with those published by van Vliet (2000), van Vliet and van Mier (2000a). The resulting deterministic size effect curve is just the same curve as before shifted to the left (recall Eq. 3). The average curve obtained with random strength field with the same autocorrelation length then unsticks to join the Weibull integral solution. Based on various parametric studies, it seems that a very good fit of the experimental results (stress–strain diagrams, the mean size effect curve shape and scatter at all sizes but A) would be obtained if $G_F = 200/16 \text{ N/m}$, the mean material strength $\mu_0 = 1.5 \times 3.2 = 4.8 \text{ MPa}$ and $m \approx 14$, a realistic value of strength scatter for concrete. The horizontal deterministic asymptotes would appear higher in Fig. 14, the asymptotic slope of statistical part would be milder

and strength scatter would be less than using the present values. Transitions would happen at smaller sizes than now.

It seems that the mean size effect as well as the statistical scatter at the same time could be explained by a combination of the ‘weak layer’, ‘deterministic-energetic’, ‘strain gradient’ and ‘statistical’ size effects together. The very thick curve in Fig. 7 of (Vořechovský 2007) (a curve denoted as 3) is the curve resulting from the combination of all three effects described here. With NLCEM modeling here, the curve would be very similar.

Finally, it can be questioned whether the crack band width is the correct parameter to represent the deterministic scaling length. Similarly the softening adjusted modulus (driven by adjusted fracture energy G_F) of a material point was designed so that a crack band occupying one band of an element’s width always dissipates the same amount of energy irrespective of the band width. Unfortunately, we are not able to model a situation where the deterministic characteristic length is greater than the statistical one (represented by the autocorrelation length in our model). This is because we cannot represent a real crack below the level of resolution of FEM discretization.

Moreover, the crack band model is not suitable when more than one crack appears in parallel, because it was primarily designed to correctly represent a single crack passing through a specimen without mesh size dependency. In our simulations it sometimes happened that at the onset of cracking the crack pattern was diffused, and the consumed energy was then probably higher than what was thought to be correct. Fortunately, localization always started soon (in terms of position on the $\sigma-\Delta u$ diagram) and the peak force we recorded was not influenced much. In our constitutive model the crack returns energy during unloading, and this supports the hypothesis that the virtual error was not high.

Both the aforementioned issues can probably be solved by using a better regularization technique to prevent spurious mesh localization; the nonlocal continuum model proposed by Pijaudier-Cabot and Bažant (1987). In this model the deterministic length is well defined by the averaging length l_a (internal length of the nonlocal continuum) over which a certain variable is averaged (based on the weight function α) (Jirásek 1998). In our eyes such a model would better represent the effect of interaction of the two lengths: deterministic l_a and statistical l_r . Another very promising option

seems to be the cohesive segments method (Remmers et al. 2003) in which the cohesive segments are inserted into finite elements as discontinuities in the displacement field by exploiting the partition-of-unity property of the shape functions.

6 Conclusions

We present a combination of nonlinear computational mechanics tools with a simulation of random fields of spatially correlated material properties in a single platform as an approach to the modeling of failure in quasibrittle materials. The performed numerical simulations of the random responses of tensile tests with dog-bone specimens with rotating boundary conditions performed by van Vliet and van Mier are in good agreement with the published data. Based on the comparison of trends of nominal strength dependency on structural size we conclude that the suggested numerical model featuring three scaling lengths is capable of capturing the most important mechanisms of failure.

In particular, we have shown that a portion of the experimentally obtained size effect can be captured at a deterministic level with the help of deterministic length represented by crack band width in our models (the smeared cracking with the crack band models are compared for a fracture-plastic and microplane material models).

Secondly, further strength dependence on size in large specimens is modeled by an autocorrelated random strength field. The important statistical length scale is introduced in the form of the autocorrelation length of the field. It is shown that the inhomogeneity of material properties over the structure in the form of an autocorrelated random strength field gives rise to imperfections that trigger fracturing in highly stressed regions of a structure. We believe that the statistical description of standard continuum helps to resolve the ill-posedness of the continuum model after the onset of localization, it being a fundamental problem. The asymptotic size effect form caused by local strength randomness is the classical Weibull power law. By random sampling of the local strength field we were also able to model the random scatter of resulting nominal strengths. Also, simple scaling rules, anchored in theoretical dimensional analysis, are suggested.

In the presented model, the complex interplay of several scaling lengths is captured at a time. Numerical simulations of localization phenomena demonstrate

that the introduction of the stochastic distribution of material properties reveal phenomena that would otherwise remain unnoticed.

Acknowledgements Authors thank to anonymous reviewers for their valuable comments that lead to many improvements of the paper. This outcome has been achieved with the financial support of the Ministry of Education, Youth and Sports, project No. MSMT 0021630519. In this undertaking, theoretical results gained in the project KJB201720902 from the Grant Agency of the Academy of Sciences of the Czech Republic were partially exploited.

References

- Barenblatt GI (1996) Scaling, self-similarity, and intermediate asymptotics No. 14 in Cambridge texts in applied mathematics. Cambridge University Press, Cambridge
- Bažant ZP, Oh BH (1983) Crack band theory for fracture of concrete. *Mater Struct* 16:155–177
- Bažant ZP, Oh BH (1986) Efficient numerical integration on the surface of a sphere. *Zeitschrift für angewandte Mathematik und Mechanik (ZAMM)* Berlin 66(1):37–49
- Bažant ZP, Pang SD (2007) Activation energy based extreme value statistics and size effect in brittle and quasibrittle fracture. *J Mech Phys Solids* 55(1):91–131
- Bažant ZP, Planas J (1998) Fracture and size effect in concrete and other quasibrittle materials. CRC Press, Boca Raton and London
- Bažant ZP, Caner FC, Carol I, Adley MD, Akers SA (2000) Microplane model M4 for concrete: I. Formulation with work-conjugate deviatoric stress. *J Eng Mech (ASCE)* 126(9):944–961
- Bažant ZP, Pang SD, Vořechovský M, Novák D (2007a) Energetic-statistical size effect simulated by SFEM with stratified sampling and crack band model. *Int J Numer Methods Eng* 71(11):1297–1320. doi:10.1002/nme.1986
- Bažant ZP, Vořechovský M, Novák D (2007b) Asymptotic prediction of energetic-statistical size effect from deterministic finite element solutions. *J Eng Mech (ASCE)* 133(2):153–162. doi:10.1061/(ASCE)0733-9399(2007)133:2(153)
- Buckingham E (1914) On physically similar systems; illustrations of the use of dimensional equations. *Phys Rev* 4(4):345–376. doi:10.1103/PhysRev.4.345
- Caner FC, Bažant ZP (2000) Microplane model M4 for concrete: II. algorithm and calibration. *J Eng Mech, ASCE* 126(9):954–961
- Carmeliet J, de Borst R (1995) Stochastic approaches for damage evolution in standard and non-standard continua. *Int J Solids Struct* 32(8–9):1149–1160. doi:10.1016/0020-7683(94)00182-V
- Carmeliet J, Hens H (1994) Probabilistic nonlocal damage model for continua with random field properties. *J Eng Mech, ASCE* 120(10): 2013–2027
- Červenka V, Pukl R (2005) Atena program documentation. Technical report, Červenka Consulting, Prague, Czech Republic. <http://www.cervenka.cz>
- Červenka J, Bažant ZP, Wierer M (2005) Equivalent localization element for crack band approach to mesh-sensitivity in microplane model. *Int J Numer Methods Eng* 62(5):700–726
- de Borst R, Gutiérrez MA, Wells GN, Remmers JJC, Askes H (2004) Cohesive-zone models, higher-order continuum theories and reliability methods for computational failure analysis. *Int J Numer Methods Eng* 60(1):289–315. doi:10.1002/nme.963
- Dyskin A, van Vliet M, van Mier J (2001) Size effect in tensile strength caused by stress fluctuations. *Int J Fract* 108:43–61
- Fisher RA, Tippett LHC (1928) Limiting forms of the frequency distribution of the largest and smallest member of a sample. *Proc Camb Philos Soc* 24:180–190
- Gutiérrez MA, de Borst R (2002) Deterministic and probabilistic material length-scales and their role in size-effect phenomena. In: Corotis R, Schuëller G, Shinozuka M (eds) Structural safety and reliability: proceedings of the eighth International Conference on Structural Safety and Reliability ICSSaR '01, A.A. Balkema Publishers, Netherlands; Swets & Zeitinger, Newport Beach, California, USA, pp 129–136, abstract page 114
- Hordijk D (1991) Local approach to fatigue of concrete. PhD thesis, Delft University of Technology, Delft, The Netherlands, ISBN 90/9004519-8
- Jirásek M (1998) Nonlocal models for damage and fracture: comparison of approaches. *Int J Solids Struct* 35(31–32):4133–4145
- Lehky D, Novák D (2002) Nonlinear fracture mechanics modeling of size effect in concrete under uniaxial tension. In: Schießl P (ed) 4th International Ph.D. Symposium in Civil Engineering, volume 2, Millpress, Rotterdam, Munich, Germany, pp 410–417
- Liu P, Der Kiureghian A (1986) Multivariate distribution models with prescribed marginals and covariances. *Probab Eng Mech* 1(2):105–111
- Mazars J, Pijaudier-Cabot G, Saouridis C (1991) Size effect and continuous damage in cementitious materials. *Int J Fract* 51:159–173
- Novák D, Lawanwisut W, Bucher C (2000) Simulation of random fields based on orthogonal transformation of covariance matrix and latin hypercube sampling. In: Schuëller (ed) International Conference on Monte Carlo Simulation MC 2000, Swets & Zeitinger, Lisse (2001), Monaco, Monte Carlo, pp 129–136
- Novák D, Bažant ZP, Vořechovský M (2003a) Computational modeling of statistical size effect in quasibrittle structures. In: Der Kiureghian A, Madanat S, Pestana JM (eds) ICASP 9, International Conference on Applications of Statistics and Probability in Civil Engineering, held in San Francisco, USA, Millpress, Rotterdam, Netherlands, pp 621–628
- Novák D, Vořechovský M, Rusina R (2003b) Small-sample probabilistic assessment—FREET software. In: Der Kiureghian A, Madanat S, Pestana JM (eds) ICASP 9, International Conference on Applications of Statistics and Probability in Civil Engineering, held in San Francisco, USA, Millpress, Rotterdam, Netherlands, pp 91–96
- Novák D, Vořechovský M, Rusina R (2006) FReET—Feasible Reliability Engineering Efficient Tool. Technical report, Brno/Červenka Consulting, Czech Republic. <http://www.freet.cz>, program documentation—Part 2—User Manual

- Pang SD, Bažant ZP, Le JL (2009) Statistics of strength of ceramics: Finite weakest-link model and necessity of zero threshold. *Int J Fract*. doi:[10.1007/s10704-009-9317-8](https://doi.org/10.1007/s10704-009-9317-8)
- Pietruszczak S, Mróz Z (1981) Finite element analysis of deformation of strain softening materials. *Int J Numer Methods Eng* 17:327–334. doi:[10.1002/nme.1620170303](https://doi.org/10.1002/nme.1620170303)
- Pijaudier-Cabot G, Bažant ZP (1987) Nonlocal damage theory. *J Eng Mech, ASCE* 113:1512–1533
- Remmers RJC, de Borst R, Needleman A (2003) A cohesive segments method for the simulation of crack growth. *Comput Mech* 31(1–2):69–77. doi:[10.1007/s00466-002-0394-z](https://doi.org/10.1007/s00466-002-0394-z)
- van Mier J, van Vliet M (2003) Influence of microstructure of concrete on size/scale effects in tensile fracture. *Eng Fract Mech* 70:2281–2306
- van Vliet M (2000) Size effect in tensile fracture of concrete and rock. PhD thesis, Delft University of Technology, Delft, The Netherlands
- van Vliet M, van Mier J (1998) Experimental investigation of size effect in concrete under uniaxial tension. In: Mihashi H, Rokugo K (eds) *FRAMCOS-3*. Aedificatio Publishers, Japan, pp 1923–1936
- van Vliet M, van Mier J (1999) Effect of strain gradients on the size effect of concrete in uniaxial tension. *Int J Fract* 95:195–219
- van Vliet M, van Mier J (2000a) Experimental investigation of size effect in concrete and sandstone under uniaxial tension. *Eng Fract Mech* 65:165–188
- van Vliet M, van Mier J (2000b) Size effect of concrete and sandstone. *Eng Fract Mech* 45:91–108
- Vashy A (1892) Sur les lois de similitude en physique. *Annales télégraphiques* 19:25–28
- Vořechovský M (2004a) Statistical alternatives of combined size effect on nominal strength for structures failing at crack initiation. In: Stibor M (ed) *Problémy lomové mechaniky IV (Problems of Fracture Mechanics IV)*, Brno University of Technology, Academy of Sciences—Institute of physics of materials of the ASCR, pp 99–106, invited lecture
- Vořechovský M (2004b) Stochastic fracture mechanics and size effect. PhD thesis, Brno University of Technology, Brno, Czech Republic
- Vořechovský M (2007) Interplay of size effects in concrete specimens under tension studied via computational stochastic fracture mechanics. *Int J Solids Struct* 44(9):2715–2731. doi:[10.1016/j.ijsolstr.2006.08.019](https://doi.org/10.1016/j.ijsolstr.2006.08.019)
- Vořechovský M (2008) Simulation of simply cross correlated random fields by series expansion methods. *Struct safety* 30(4):337–363. doi:[10.1016/j.strusafe.2007.05.002](https://doi.org/10.1016/j.strusafe.2007.05.002)
- Vořechovský M, Chudoba R (2006) Stochastic modeling of multi-filament yarns: II. Random properties over the length and size effect. *Int J Solids Struct* 43(3–4):435–458. doi:[10.1016/j.ijsolstr.2005.06.062](https://doi.org/10.1016/j.ijsolstr.2005.06.062)
- Vořechovský M, Novák D (2004) Modeling statistical size effect in concrete by the extreme value theory. In: Walraven J, Blaauwendraad J, Scarpas T, Snijder B (eds) *5th International Ph.D. Symposium in Civil Engineering*, held in Delft, The Netherlands, A.A. Balkema Publishers, London, UK, vol 2, pp 867–875
- Vořechovský M, Bažant ZP, Novák D (2005) Procedure of statistical size effect prediction for crack initiation problems. In: Carpinteri A (ed) *ICF XI 11th International Conference on Fracture*, held in Turin, Italy, Politecnico di Torino, pp CD-ROM proc, abstract page 1166
- Vořechovský M, Chudoba R, Jeřábek J (2006) Adaptive probabilistic modeling of localization, failure and size effect of quasi-brittle materials. In: Soares et al (eds) *III European Conference on Computational Mechanics (ECCM-2006)*, held in Lisbon, Portugal, National Laboratory of Civil Engineering, Springer, p 286 (abstract), full papers on CD-ROM
- Weibull W (1939) The phenomenon of rupture in solids. *Roy Swedish Inst Eng Res (Ingenioersvetenskaps Akad Handl)* Stockholm 153:1–55